Low Hydrogen Solubility in Clay Interlayers Limits Gas Loss in Hydrogen Geological Storage

Tuan A. Ho[1*], Carlos F. Jove-Colon[2], and Yifeng Wang[2]

[1]*Geochemistry Department, Sandia National Laboratories, Albuquerque, NM 87185, USA*
[2]*Nuclear Waste Disposal Research and Analysis Department, Sandia National Laboratories, Albuquerque, NM 87185, USA*
*****Corresponding author: taho@sandia.gov*

Electrical Supplementary Information

1. Metadynamics molecular simulations

In Fig. 1A, we provide a representative simulation snapshot used to calculate the PMF of a H_2 molecule moving along the z direction from vacuum into bulk water. The reaction coordinate of the PMF is the z position of the H_2 molecule. The PMF calculation is performed using well-tempered metadynamics.[1] In a standard metadynamics calculation[2] a Gaussian potential $V(r,t) = \omega\, e^{-\frac{[r-r(t)]^2}{2\sigma^2}}$ (r is the reaction coordinate, t is the time, ω and σ are the Gaussian height and width) is deposited at every time interval τ to the potential energy landscape to allow the system to explore the full energy landscape. When the modified free energy (potential energy plus the Gaussian potential) becomes constant along the reaction coordinate, the PMF is the negative of the sum of all Gaussians deposited. In a standard metadynamics simulation, it is difficult to decide when to stop the simulation because the free energy does not converge but fluctuates around the correct result. In addition, continuing a simulation run might force the system to a configuration that is not physically relevant.[1] To tackle these problems, well-tempered metadynamics were developed.[1] In a well-tempered metadynamics calculation, a Gaussian potential has the form of $V'(r,t) = \omega e^{-\frac{V(r,t)}{k_B\Delta T}} e^{-\frac{[r-r(t)]^2}{2\sigma^2}}$, where ΔT is a tunable temperature-like parameter that controls how quickly the Gaussian height, $\omega e^{-\frac{V(r,t)}{k_B\Delta T}}$, reduces as the Gaussian is being deposited, k_B is the Boltzmann constant. The height of a Gaussian $\omega e^{-\frac{V(r,t)}{k_B\Delta T}}$ decreases with simulation time, which allows a PMF to converge more smoothly. For a well-tempered metadynamics simulation, the choice of ω, σ, τ, and ΔT decides the efficiency and convergence of a calculation. We report in Fig. S1 the PMF as a function of time to demonstrate the convergence of the PMF calculation and ω, σ, τ, and ΔT parameters.

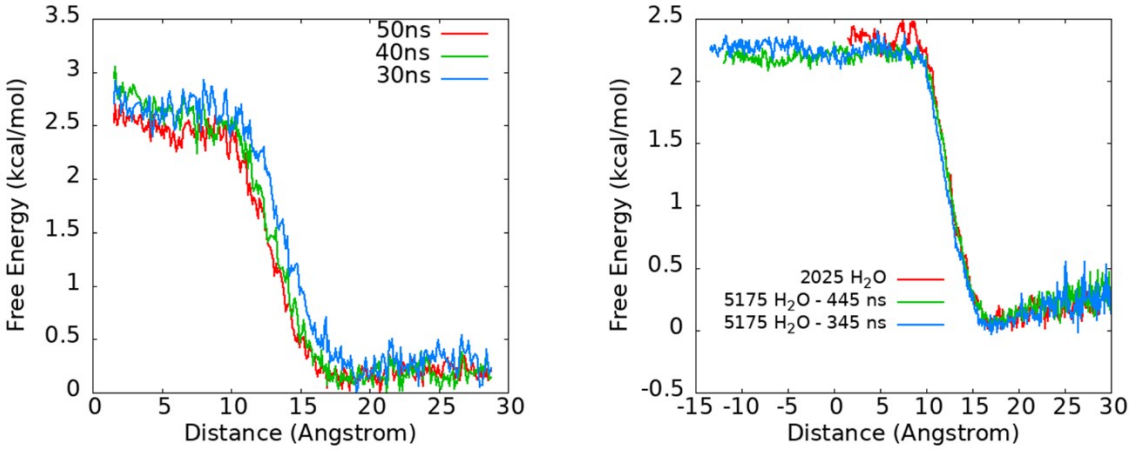

Fig. S1. Left: The potential of mean force for H_2 dissolution in bulk water as a function of simulation time. The results indicate the convergence of the PMF calculation. The temperature is 323 K. The PMF is calculated with Gaussian ω = 1 kcal/mol, σ = 2 Å, ΔT =3000 K, and τ = 1000 timesteps. **Right**: Comparison of the PMF profiles at 300K when there are 2025 and 5175 water molecules in the simulation box.

There are 2025 water molecules and 1 H_2 molecule in a 50×50×70 Å^3 simulation box in Fig. 1A. We implemented a SPC water model model[3] and 3-site H_2 model[4] which reproduces very well the solubility of H_2 in water. The Lennard-Jones (LJ) potential is expressed as: $V_{LJ} = 4\varepsilon\left[\left(\frac{\sigma}{r}\right)^{12} - \left(\frac{\sigma}{r}\right)^{6}\right]$, where r is the distance between two atoms, ε and σ are the depth of the potential energy well and the distance at which the LJ potential is zero, respectively. LJ interactions among atoms are calculated using the Lorentz-Berthelot mixing rules $\varepsilon_{ij} = \sqrt{\varepsilon_{ii}\varepsilon_{jj}}$ and $\sigma_{ij} = (\sigma_{ii} + \sigma_{jj})/2$. Short range interactions are calculated using a cut-off distance of 10 Å. Long range electrostatic interactions are calculated using the PPPM (particle-particle-particle-mesh) solver.[5] All simulations are performed at 300 or 323 K using the Nose-Hoover thermostat,[6] and the timestep is 1 fs.

2. H_2 model selection

Since the H_2 interaction with water is very important in this study, we aim to reproduce the solubility of H_2 in water. We calculate the H_2 solubility as a function of gas pressure using the model in Fig. S2 (left). There are 2025 water molecules and a certain number of H_2 molecules in a simulation box of 50×50×70 Å^3. We implement a SPC water model model.[3] The Lennard-Jones (LJ) potential is expressed as: $V_{LJ} = 4\varepsilon\left[\left(\frac{\sigma}{r}\right)^{12} - \left(\frac{\sigma}{r}\right)^{6}\right]$, where r is the distance between two atoms, ε and σ are the depth of the potential energy well and the distance at which the LJ potential is zero, respectively. LJ interactions among atoms are calculated using the Lorentz-Berthelot mixing rules $\varepsilon_{ij} = \sqrt{\varepsilon_{ii}\varepsilon_{jj}}$ and $\sigma_{ij} = (\sigma_{ii} + \sigma_{jj})/2$. The system in Fig. S2 is simulated in an NVT simulation with tempearture of 323K. The simulation is conducted for about 100 ns. We calculate the density of

H_2 in the gas phase to determine the pressure using ideal gas law. The amount of H_2 in the water phase is used to determine the solublity.

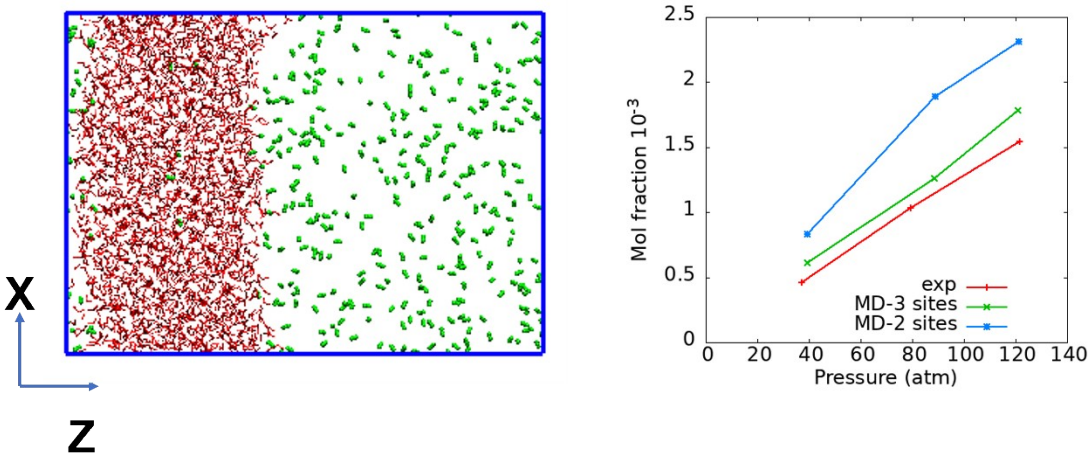

Fig S2. Simulation system (left) including water (red) and hydrogen (green) molecules used to determine the solubility of H_2 in bulk water (right) at 323 K. The experimental value is from ref.[7]

Two hydrogen models (2-sites[8] and 3-sites[4]) are considered in this work. In the two LJ sites model, each H atom is a LJ sphere (σ = 0.259 nm and ε = 0.02484 kcal/mol) and H-H distance is 0.074 nm.[8] This model were used to study H_2 adsorption onto graphitic materials, MOFs, and zeolite.[8 9, 10] This model does not include electrostatic interactions leading to underestimation of the strength of H_2 interaction with open metal site in MOFs. The 3-site model contains the center-of-mass (COM) LJ site and has partial charges located on the COM site and the positions of the H atoms.[4] Because the 3-sites model has partial charge sites along with a LJ site (overall they are neutral) it has the ability to capture the polarization. The simulation results in Fig. S2 (right) indicate that the 3-sites model is better than the 2-sites model at predicting the solubility of H_2 in water.[4] The 3-sites model will be used to investigate the H_2 intercalation into the clay interlayers.

3. Clay layer construction, force fields, and PMF calculation details

3.1 Clay layer construction

The system in Fig. 2A and Fig. S3 includes a clay layer with patch-wise charge distribution. When applying periodic boundary condition in the z direction, water (red) is confined between two identical clay layers.

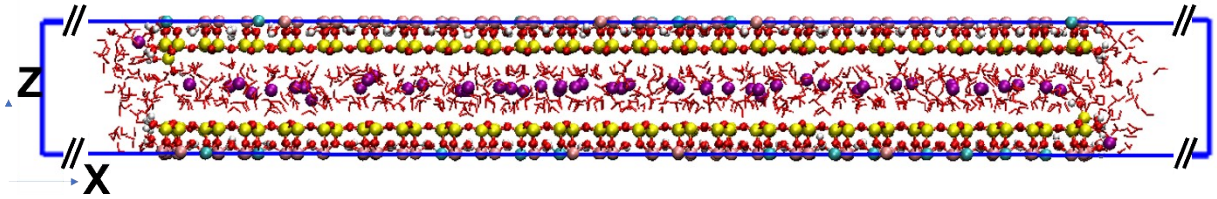

Fig. S3. Water confined in two identical clay layers through applied periodic boundary condition. The simulation box size is 200×31.06×15 Å^3. The 104 Å long ribbon clay layer has 2916 atoms. There are 715 water molecules, including those at the clay edge, 1 H_2 molecule, and 52 Na^+ ions .

The method to build the clay layer in Fig. 2A can be found in our previous work.[11] Briefly, a pyrophyllite layer was cleaved on the (0 1 0) face.[12, 13] The resultant broken bonds were fixed by adding –OH groups or –H atoms so that (i) each Si atom at the edge coordinates with 4 oxygen atoms and (ii) each edge Al atom coordinates with 5 oxygen atoms. In a solution, a 5-coordinated edge Al atom usually coordinates with a water molecule to complete its 6-coordinated configuration.[14, 15] After constructing the pyrophyllite layer with edges, we substituted some Al atoms in the octahedral sheet with Mg atoms to obtain the montmorillonite (MMT) layer with Mg:Al ratio of 0.75: 3.25. This substitution is subjected to two constraints. First, no substitution site is adjacent to another in the octahedral sheet.[16] Second, the Mg:Al ratio is smaller than 0.2 at the edge.[17] The distribution of Mg atoms in the Al octahedral sheet, which determines the charge distribution, is either patch-wise or random in our simulations (Fig. S4). The negative charge due to the substitution is balanced by Na^+ ions in the interlayers. Enough water molecules are added into the interlayers to obtain the 1W or 2W hydration state.

Macroscopically, MMT is a hydrophilic material (i.e., water wets MMT surfaces).[18] Microscopically (e.g., at the molecular level), an MMT surface can have both hydrophobic sites (e.g., siloxane rings underlain by octahedral Al atoms) and hydrophilic sites (e.g., siloxane rings underlain by Mg atoms that substitute for Al atoms, and occupied by counter ions in the interlayers).[19, 20] Simulation work also concluded that bare smectite surfaces (e.g., without the counter ions) are either hydrophobic or moderately hydrophilic. The macroscopically hydrophilic character of smectite surface is almost entirely due to charge balancing cations.[21]

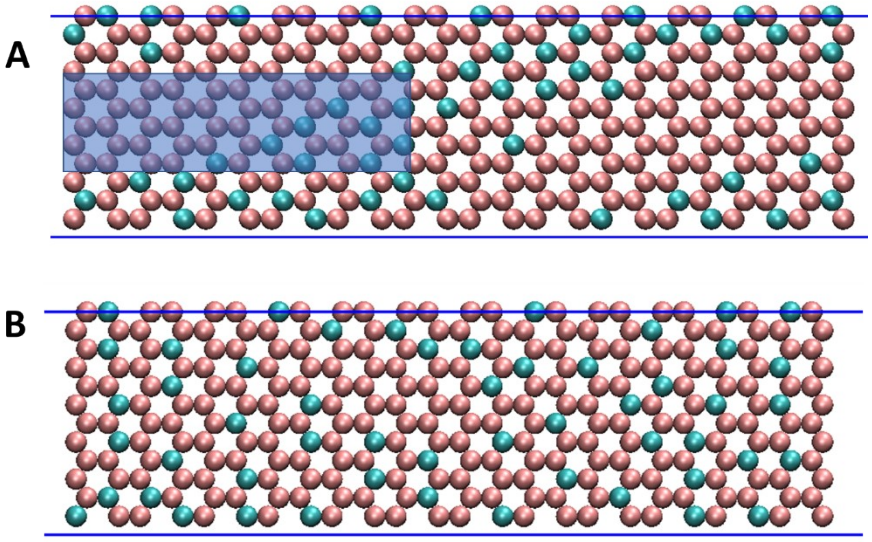

Fig. S4 Patch-wise (**A**) and random (**B**) charge distributions in the octahedral sheet of a clay layer. Pink spheres are Al atoms, cyan spheres are the Mg atoms that substitute for Al atoms. The PMF in Fig. 2 is calculated within the shaded region in Fig. S4A.

3.2 Force fields

The Na-MMT layer/particle is simulated by the ClayFF force field,[22] with additional Si-O-H and Al-O-H angle terms describing the edges.[23, 24] The interactions of Na^+ ions with bridging oxygen of surface (*ob* type in ClayFF force field) are also modified according to our previous work.[25] Water molecules are simulated using a flexible SPC water model,[3] and Na^+ ion is modeled by the force field proposed by Dang and Smith.[26]

After selecting the 3-sites H_2 model, SPC water, and ClayFF force field, we need to ensure that the interaction between H_2 and clay layer is appropriate. We first perform the molecular dynamics simulation for the system including hydrogen molecules confined in the pyrophyllite nanopore (Fig. S5, top left) using the using the Lorentz-Berthelot mixing rules $\varepsilon_{ij} = \sqrt{\varepsilon_{ii}\varepsilon_{jj}}$ and $\sigma_{ij} = (\sigma_{ii} + \sigma_{jj})/2$ for pair-wise interactions. We select pyrophyllite instead of MMT in this calculation because MMT is built from pyrophyllite structure with octahedral substitution. In an idea case we need to consider the interaction of H_2 with counterions (e.g., Na^+) and the Mg sites. However, with water molecules closely coordinate with Na^+ ions and accumulate near charge sites (Mg), H_2 will not interact directly with those sites. The simulation is performed in the NVT ensample with T= 300 K. Density profile (green line) of hydrogen in pyrophyllite nanopore is reported in Fig. S5, bottom. We compare this density profile with that obtained from *ab initio* MD (AIMD) calculation using the model in Fig. S5, top right. The AIMD calculation is performed using VASP.[27] The exchange-correlation energy was calculated using GGA with the PBE parameterization.[28] The interaction between valence electrons and ionic cores was described by the projector augmented wave (PAW) method.[29] The plane-wave cutoff energy for the electronic wavefunctions was set to 400 eV. Temperature is set at 300 K. The comparison of the density profile obtained from MD and AIMD indicates that the original interaction between H_2 and pyrophyllite does not reproduce the structure of H_2 in the pyrophyllite nanopore.

To better reproduce the H_2 density profile using MD simulation, we decide to modify the interaction parameter between H_2 and bridging oxygen atom of the pyrophyllite surface, i.e., the *ob* atom type in the CLAYFF force field.[1] According to the Lorentz-Berthelot mixing rule the ε_{ij} and σ_{ij} for H atom and *ob* are 0.106464 kcal/mol and 0.306276 nm. We modify them to become 0.08 kcal/mol and 0.325 nm. The density profile obtained for the modified MD model (blue line, Fig S5, bottom) is comparable with the density profile obtained from AIMD simulation.

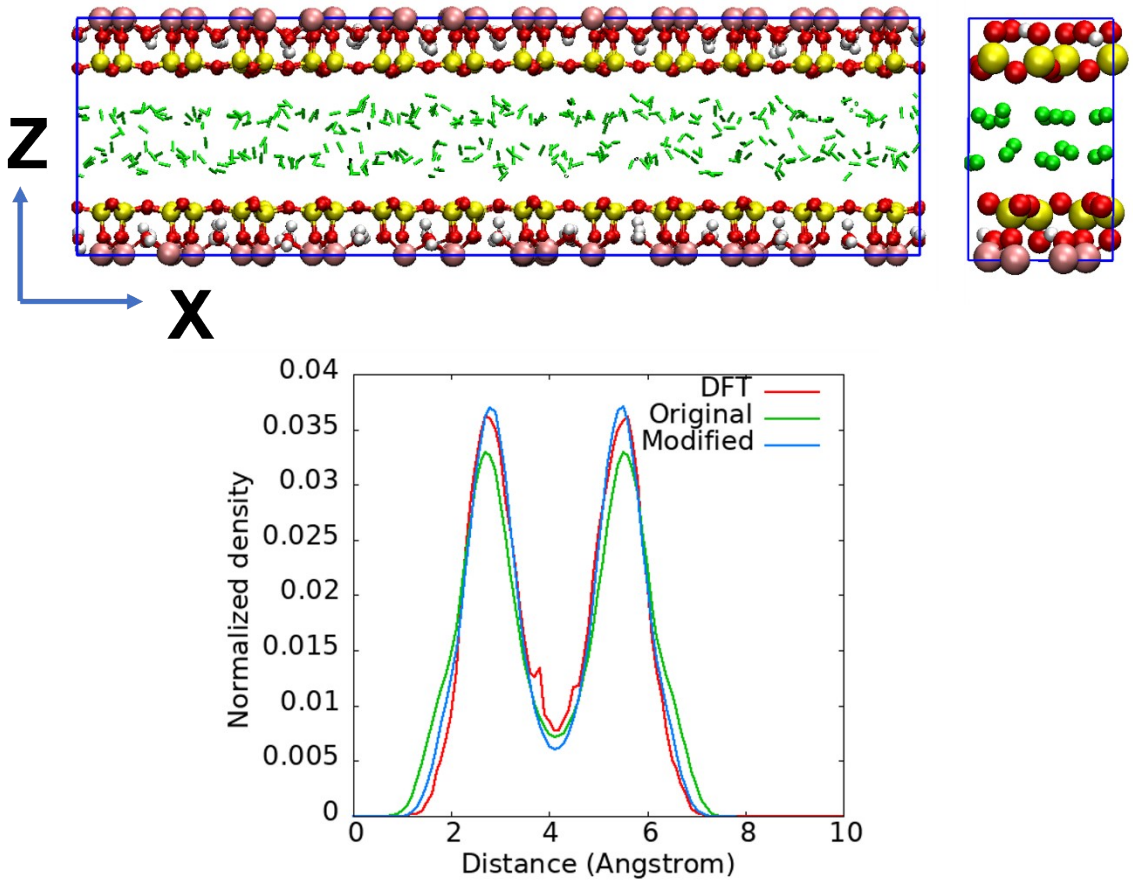

Fig. S5. The MD (top left) and DFT (top right) models used to benchmark the interaction of H_2 with pyrophyllite. The simulation box size for DFT model is 5.16×8.96×15 Å^3, including a pyrophyllite layer and 10 hydrogen molecules. The MD model is 36 times larger than the DFT model. Density profile of H_2 in the pyrophyllite nanopore (bottom).

3.3 PMF calculation details for Fig 2.

During the PMF calculation, the H_2 molecule moves along the x direction (Fig. 2A and Fig. S3), i.e., the reaction coordinate of the PMF is the x position of the H_2 molecule. The H_2 molecule is also restricted to move inside the blue region of the xy plane highlighted in Fig. 2B using a harmonic constraint $E=k\,(y - y_o)^2$ with spring constant of k = 0.1 kcal/mol in the y direction (y_o is the y coordinate of H_2 molecule at the center of the blue region). The position of the H_2 molecule in the xy plane during the PMF calculation is reported in Fig. S6. Note that the system in Fig. 2A is just a part of the system in Fig. S3; i.e., we did not conduct the PMF for H_2 intercalation into a full length of the system in Fig. S3. The H_2 molecule is limited to move inside the blue region in Fig. 2B and Fig. S4A. The clay layer and water molecules are equilibrated before introducing the H_2 molecule to the vacuum space for the PMF calculation using well-tempered metadynamics.[1] We report in Fig. S7 the PMF as a function of time to demonstrate the convergence of the PMF calculation for Fig. 2C and ω, σ, τ, and ΔT parameters.

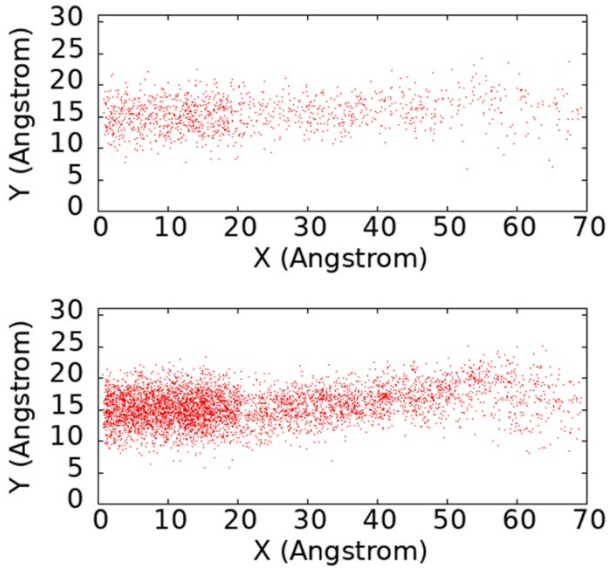

Fig. S6. Positions of the H_2 molecule on the xy plane during the PMF calculation for Fig. 2 for 2W (top) and 1W (bottom) systems.

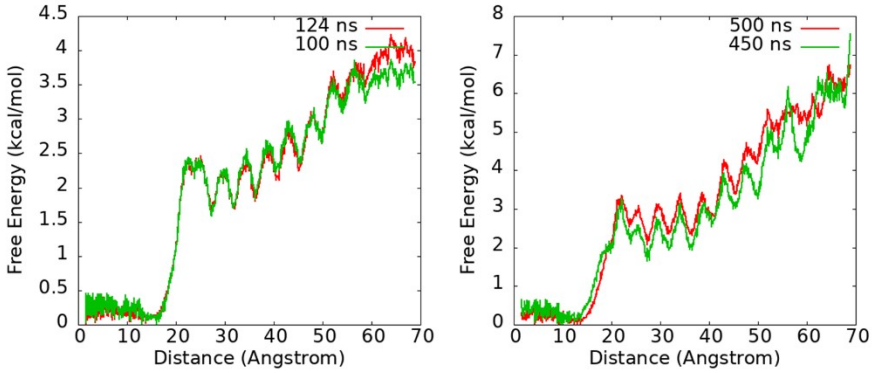

Fig. S7. The PMF of H_2 intercalation into 2W (left) and 1W (right) systems presented in Fig. 2 as a function of simulation time. These results demonstrate the convergence of the PMF calculation. The temperature is 323 K. The PMF is calculated with Gaussian ω = 1.5 kcal/mol, σ = 2 Å, ΔT =1000 K, and τ = 1000 timesteps.

4. PMF calculation details for Fig. 3.

The PMF calculation is carried out while the H_2 molecule can only enter the bottom pore by constraining the H_2 z coordinate at the bottom pore center with a harmonic spring constant of 1 kcal/mol. The H_2 molecule is also restricted to move in the blue region on the xy plane with a harmonic spring constant of 0.2 kcal/mol in the y direction.

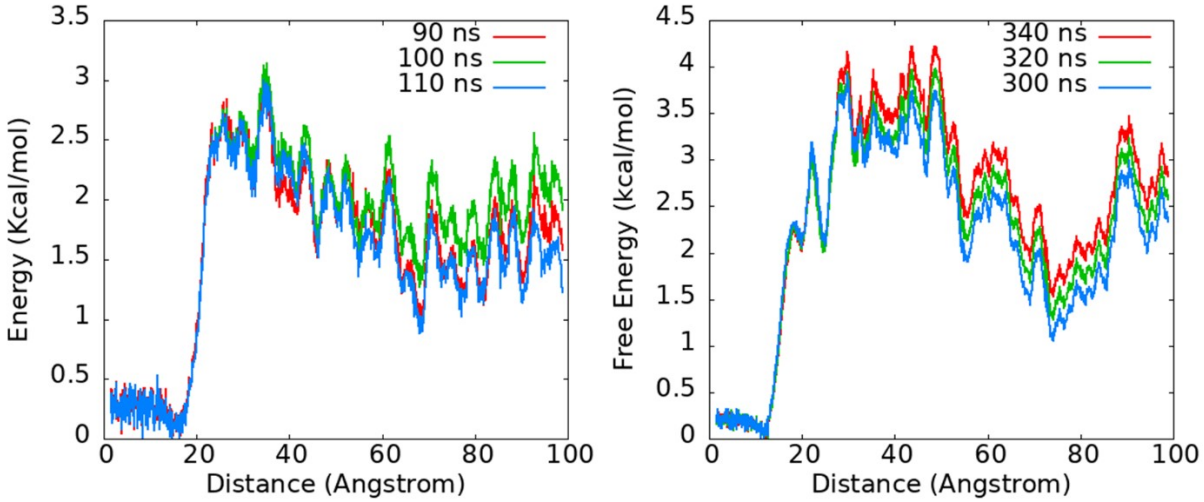

Fig. S8. The PMF of H_2 intercalation into 2W (left) and 1W (right) systems presented in Fig. 3 as a function of simulation time. These results demonstrate the convergence of the PMF calculation. The temperature is 323 K. The PMF is calculated with Gaussian ω = 1.5 kcal/mol, σ = 2 Å, ΔT =1000 K, and τ = 1000 timesteps.

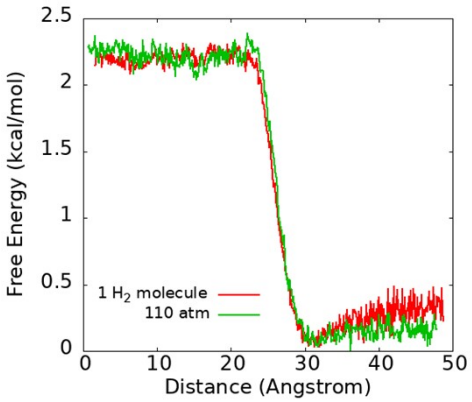

Fig. S9. Comparison of the PMF profiles at 300K when inserting a hydrogen molecule into bulk water at different pressure (vacuum vs. 110 atm H_2 pressure). 5175 water molecules is used in this simulation.

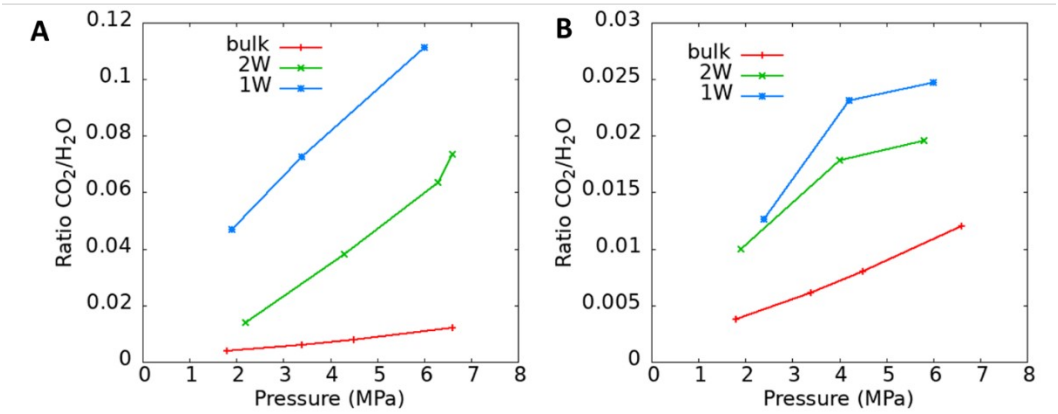

Fig. S10. Comparison of CO_2/H_2O ratio in bulk water (red) with that in confined water for 2W (green) and 1W hydrated (blue) clay interlayers for patch-wise (**A**) and random charge distribution (**B**). These results are from our previous work.[30]

Reference

1. Barducci, A.; Bussi, G.; Parrinello, M. *Phys Rev Lett* **2008,** 100, (2), 020603.
2. Laio, A.; Parrinello, M. *Proceedings of the National Academy of Sciences* **2002,** 99, (20), 12562-12566.
3. Teleman, O.; Jonsson, B.; Engstrom, S. *Mol Phys* **1987,** 60, (1), 193-203.
4. Lopez-Lazaro, C.; Bachaud, P.; Moretti, I.; Ferrando, N. *Bulletin de la Société Géologique de France* **2019,** 190, (1).
5. Hockney, R. W.; Eastwood, J. W., *Computer simulation using particles*. Taylor & Francis Group, LLC.: New York, 1988; p 564.
6. Nose, S. *Mol Phys* **1984,** 52, (2), 255-268.
7. Chabab, S.; Théveneau, P.; Coquelet, C.; Corvisier, J.; Paricaud, P. *International Journal of Hydrogen Energy* **2020,** 45, (56), 32206-32220.
8. Cracknell, R. F. *Phys Chem Chem Phys* **2001,** 3, (11), 2091-2097.
9. Salles, F.; Kolokolov, D. I.; Jobic, H.; Maurin, G.; Llewellyn, P. L.; Devic, T.; Serre, C.; Ferey, G. *The Journal of Physical Chemistry C* **2009,** 113, (18), 7802-7812.
10. Kumar, A. V. A.; Jobic, H.; Bhatia, S. K. *The Journal of Physical Chemistry B* **2006,** 110, (33), 16666-16671.
11. Ho, T. A.; Criscenti, L. J.; Greathouse, J. A. *J Phys Chem Lett* **2019,** 10, (13), 3704.
12. Lavikainen, L. P.; Hirvi, J. T.; Kasa, S.; Schatz, T.; Pakkanen, T. A. *Theoretical Chemistry Accounts* **2015,** 134, (9), 112.
13. Harvey, J. A.; Johnston, C. T.; Criscenti, L. J.; Greathouse, J. A. *Chemical Communications* **2019,** 55, (24), 3453-3456.
14. Ho, T. A.; Greathous, J. A.; Lee, A. S.; Criscenti, L. J. *Langmuir* **2018,** 34, (20), 5926-5934.
15. Ho, T. A.; Greathouse, J. A.; Wang, Y.; Criscenti, L. J. *Sci Rep-Uk* **2017,** 7, (1), 15286.
16. Loewenstein, W. *American Mineralogist* **1954,** 39, (1-2), 92-96.
17. Newton, A. G.; Kwon, K. D.; Cheong, D.-K. *Minerals* **2016,** 6, (2), 25.
18. Ho, T. A.; Wang, Y. *ACS Applied Materials & Interfaces* **2021,** 13, (34), 41330-41338.
19. Ho, T. A.; Coker, E. N.; Jové-Colón, C. F.; Wang, Y. *Nano Lett* **2022,** 22, (7), 2740-2747.
20. Ngouana, B. F.; Kalinichev, A. G. *J Phys Chem C* **2014,** 118, (24), 12758-12773.
21. Szczerba, M.; Kalinichev, A. G.; Kowalik, M. *Appl Clay Sci* **2020,** 188, 105497.
22. Cygan, R. T.; Liang, J. J.; Kalinichev, A. G. *J Phys Chem B* **2004,** 108, (4), 1255-1266.

23. Pouvreau, M.; Greathouse, J. A.; Cygan, R. T.; Kalinichev, A. G. *J. Phys. Chem. C* **2017,** 121, 14757-14771.
24. Pouvreau, M.; Greathouse, J. A.; Cygan, R. T.; Kalinichev, A. G. *The Journal of Physical Chemistry C* **2019**, 11628–11638.
25. Ho, T. A.; Criscenti, L. J.; Greathouse, J. A. *The Journal of Physical Chemistry Letters* **2019,** 10, (13), 3704-3709.
26. Smith, D. E.; Dang, L. X. *J Chem Phys* **1994,** 100, (5), 3757-3766.
27. Kresse, G.; Furthmüller, J. *Phys Rev B Condens Matter* **1996,** 54, (16), 11169-11186.
28. Perdew, J. P.; Burke, K.; Ernzerhof, M. *Phys Rev Lett* **1996,** 77, (18), 3865-3868.
29. Blöchl, P. E. *Physical Review B* **1994,** 50, (24), 17953-17979.
30. Ho, T. A.; Wang, Y.; Rempe, S. B.; Dasgupta, N.; Johnston, C. T.; Xu, G.; Zwier, T. S.; Mills, M. *The Journal of Physical Chemistry Letters* **2023,** 10.1021/acs.jpclett.3c00291.